



1

2

3

4

**Development and evaluation of a system of proxy data assimilation for
paleoclimate reconstruction**

5

6

7

8

By

9

10

Atsushi Okazaki¹ and Kei Yoshimura²

11

12

¹RIKEN Advanced Institute for Computational Science, Japan

13

²Atmosphere and Ocean Research Institute, University of Tokyo, Japan

14

15

16

17

18

19

Submitted to Climate of the Past

20

Submitted in November, 2016

21

22

23 Corresponding author: Atsushi Okazaki, RIKEN Advanced Institute for Computational
24 Science, 7-1-26 Minatojima-minami-machi, Chuo-ku, Kobe, Hyogo 650-0047, Japan
25 (atsushi.okazaki@riken.jp)



26

Abstract

27 Data assimilation (DA) has been successfully applied in the field of paleoclimatology
28 to reconstruct past climate. However, data reconstructed from proxies have been
29 assimilated, as opposed to the actual proxy values. This banned to fully utilize the
30 information recorded in the proxies.

31 This study examined the feasibility of proxy DA for paleoclimate reconstruction.
32 Isotopic proxies ($\delta^{18}\text{O}$ in ice cores, corals, and tree-ring cellulose) were assimilated into
33 models: an isotope enabled general circulation model (GCM) and forward proxy models,
34 using offline data assimilation.

35 First, we examined the feasibility using an observation system simulation experiment
36 (OSSE). The analysis showed a significant improvement compared with the first guess in
37 the reproducibility of isotope ratios in the proxies, as well as the temperature and
38 precipitation fields, when only the isotopic information was assimilated. The accuracy for
39 temperature and precipitation was especially high at low latitudes. This is due to the fact
40 that isotopic proxies are strongly influenced by temperature and/or precipitation at low
41 latitudes, which, in turn, are modulated by the El Niño-Southern Oscillation (ENSO) on
42 interannual timescales. The proxy temperature DA had comparable or higher accuracy
43 than the reconstructed temperature DA.

44 The proxy DA was compared with real proxy data. The reconstruction accuracy was
45 decreased compared to the OSSE. In particular, the decrease was significant over the
46 Indian Ocean, eastern Pacific, and the Atlantic Ocean where the reproducibility of the
47 proxy model was lower. By changing the experimental design in a stepwise manner, the
48 decrease in accuracy was found to be attributable to the misrepresentation of the models.
49 In addition, the accuracy was also dependent on the number and/or distribution of the
50 proxies to be assimilated. Thus, to improve climate DA, it is necessary to enhance the
51 performance of models, as well as to increase the number of proxies.

52



53 **1. Introduction**

54 Knowledge of past conditions is crucial for understanding long-term climate
55 variability. Historically, two approaches have been used to reconstruct paleoclimate; one
56 based on the empirical evidence contained in proxy data, and the other based on
57 simulation with physically-based climate models. Recently, an alternative approach
58 combining proxy data and climate simulations using a data assimilation (DA) technique
59 has emerged. DA has long been used for forecasting weather and is a well-established
60 method. However, the DA algorithms used for weather forecasts cannot be directly
61 applied to paleoclimate due to the different temporal resolution, spatial extent, and type
62 of information contained within observation data (Widmann et al., 2010). The temporal
63 resolution and spatial distribution of proxy data are significantly lower (seasonal at best)
64 and sparser than the present-day observations used for weather forecasts, and the
65 information we can get does not measure the direct states of climate (e.g., temperature,
66 wind, pressure, etc.), but represents proxies of those states (e.g., tree-ring width, isotopic
67 composition in ice sheets, etc.). Thus, DA applied to paleoclimate is only loosely linked
68 to the methods used in the more mature field of weather forecasting, and it has been
69 developed almost independently from them.

70 Several DA methods have been proposed for paleoclimate reconstruction (von Storch



71 et al., 2000; van der Schrier et al., 2005; Dirren and Hakim, 2005; Goosse et al., 2006;
72 Bhend et al., 2012; Dubinkina and Goosse, 2013; Steiger et al., 2014), and paleoclimate
73 studies using DA have successfully determined the mechanisms behind climate changes
74 (Crespin et al., 2009; Goosse et al., 2010; 2012; Mathiot et al., 2013). In previous studies,
75 the variables used for assimilation have been data reconstructed from proxies (e.g.,
76 surface air temperature) because observation operators or forward models for proxies
77 have not been readily available. Hereafter, the DA method that assimilates reconstructed
78 data from proxies is referred to as reconstructed DA. Recently, proxy modelers have
79 developed and evaluated several forward models for stable water isotopic proxies (e.g.,
80 Dee et al., 2015 and references therein). In this study, we attempted to assimilate proxy
81 data directly for the first time.

82 The main advantage of proxy DA over reconstructed DA is the richness of information
83 used for assimilation. In previous studies, only a single reconstructed field was
84 assimilated. However, proxies are influenced by multiple variables. Hence, the
85 assimilation of a single variable does not use the full information recorded in the proxies.

86 The reconstruction method itself also limits the amount of information. The most
87 commonly-used climate reconstruction is an empirical and statistical method that relies
88 on the relationships between climate variables and proxies observed in present-day



89 observations. These relationships are then applied to the past climate proxies to
90 reconstruct climate prior to the instrumental period. Most of the studies using this
91 approach assume that the relationship is linear. However, this assumption imposes
92 considerable limitations in which specific climate proxies can be used, and proxies that
93 do not satisfy the assumption have generally been omitted (e.g., PAGES 2k Consortium,
94 2013). Because information on paleoclimate is scarce, it is desirable to use as much
95 information as possible.

96 Furthermore, the reconstruction method also limits the quality of information
97 provided. The method also assumes stationarity of the relationship between the climate
98 and the proxies. However, this assumption has been shown to be invalid for some cases
99 (e.g., Schmidt et al. 2007; LeGrande and Schmidt, 2009). In the case of reconstructed DA,
100 the assimilation of such erroneous data would provide unrealistic results. In the case of
101 proxy DA; however, the accuracy of the assimilation is expected to be unchanged,
102 provided the model can correctly simulate the non-stationarity.

103 The concept of proxy data assimilation is not new, and has been proposed in previous
104 studies (Hughes and Ammann, 2009; Evans et al., 2013; Yoshimura et al., 2014; Dee et
105 al., 2015). Yoshimura et al. (2014) demonstrated that the accuracy of the simulation
106 results increased following assimilation of the stable water isotope ratios of vapor for



107 current weather forecasting. They performed an observation system simulation
108 experiment (OSSE) assuming that isotopic observations from satellites were available
109 every six hours. Because the isotope ratio of water is one of the most frequently used
110 climate proxies, this represents a significant first step toward improving the performance
111 of proxy data assimilation in terms of identifying suitable variables for assimilation.
112 However, it is not yet clear whether it is feasible to constrain climate only using isotopic
113 proxies whose temporal resolution and spatial coverage are much longer and sparser than
114 those of the specific study.

115 This study examined the feasibility of isotopic proxy DA for the paleoclimate
116 reconstruction on the interannual timescale. Because the study represents the first attempt
117 to assimilate isotopic variables on this timescale, we adopted the framework of an OSSE,
118 as in previous climate data assimilations (Annan and Hargreaves, 2012; Bhend et al.,
119 2012; Steiger et al., 2014). After the evaluation of proxy DA in the idealized way, we
120 conducted the study with “real” proxy DA. We investigated which factors decreased or
121 increased the accuracy of the proxy DA.

122 In this study, we used only oxygen isotopes (^{18}O) as proxies. The isotope ratio is
123 expressed in delta notation ($\delta^{18}\text{O}$) relative to Vienna Standard Mean Ocean Water
124 (VSMOW) throughout the manuscript. If the original data were expressed in delta



125 notation relative to Vienna Pee Dee Belemnite (VPDB), they were converted to the
126 VSMOW scale.

127 This paper is structured as follows. In the following section, the data assimilation
128 algorithm, models, data, and experimental design are presented. Section 3 shows the
129 results of the idealized experiment. Section 4 gives the results of the real proxy DA. The
130 Discussion is presented in Section 5. Finally, we present our conclusions in Section 6.

131

132 **2. Materials and methods**

133 **2.1. Data assimilation algorithm**

134 We used the so-called “offline data assimilation” algorithm to assimilate time-
135 averaged data. In offline data assimilation, the analysis procedure is not cycled to the
136 simulation (Bhend et al., 2012); thus, the background ensembles can be constructed from
137 existing climate model simulations (Huntley and Hakim, 2010; Steiger et al., 2014). As
138 such, we can assimilate data with any temporal resolution coarser than the model outputs.
139 In this study, we focused on annual data assimilation. Following the procedure proposed
140 by Steiger et al. (2014), the background ensemble was taken from part of a single climate
141 model simulation, where the ensemble members were individual years instead of
142 independent model simulations. This algorithm was selected to reduce computational



143 costs. This simplification was valid because the interannual variability in a single run was
144 inherently indistinguishable from the variability in the annual mean within the ensemble
145 of simulations in which the initial conditions were perturbed. Thus, the background
146 ensembles were the same for all of the reconstruction years and did not contain any year-
147 specific boundary conditions and forcing information; hence, the background error
148 covariance was constant over time. Therefore, this study did not consider non-stationarity
149 between the proxies and climate. Despite the limitations of the algorithm used in this
150 study, it should be noted that the proxy DA could address non-stationarity by changing
151 the algorithm. We return to this point in Section 5.

152 To control spurious long-distance correlations due to sampling errors, a localization
153 function proposed by Gaspari and Cohn (1999) with a scale of 12,000 km was used. The
154 detailed procedure used for the algorithm is described in Steiger et al. (2014).

155

156 **2.2. Models**

157 Isotope ratios recorded in ice cores, corals, and tree-ring cellulose were assimilated.
158 To assimilate these variables, forward models for the variables are required. We used the
159 forward model developed by Liu et al. (2013; 2014) for corals, and Roden et al. (2000)
160 for tree-ring cellulose. We assumed that the isotopic composition of ice cores was the



161 same as that of precipitation at the time of deposition. Note that, in reality, the isotope
162 ratio recorded in ice cores is not always equal to that in precipitation due to post-
163 depositional processes (e.g., Schotterer et al., 2004). Because detailed models that
164 explicitly simulate the impact of all the processes involved in determining the value of
165 the ratio are not yet available, we used the isotope ratio in precipitation for that in ice
166 cores to avoid adding unnecessary noise.

167 The isotopic composition in precipitation was simulated using an atmospheric general
168 circulation model (GCM) into which the isotopic composition of vapor, cloud water, and
169 cloud ice are incorporated as prognostic variables. The model explicitly simulates the
170 isotopic composition with all the details of the fractionation processes combined with
171 atmospheric dynamics and thermodynamics, and hydrological cycles. Hence, the model
172 simulates the isotopic composition consistent with the modeled climate. Although many
173 such models have been developed previously (Joussaume et al., 1984, Jouzel et al., 1987;
174 Hoffmann et al., 1998; Noone and Simmonds, 2002; Schmidt et al., 2005; Lee et al., 2007;
175 Yoshimura et al., 2008; Risi et al., 2010; Werner et al., 2011), we used a newly-developed
176 model (Okazaki et al., in prep.) based on MIROC5 (Watanabe et al. 2010). The spatial
177 resolution was set to T42 (approximately 280 km) with 40 vertical layers.

178 The variability in $\delta^{18}\text{O}$ recorded in coral skeleton aragonite ($\delta^{18}\text{O}_{\text{coral}}$) depends on the



179 calcification temperature and local $\delta^{18}\text{O}$ in sea water ($\delta^{18}\text{O}_{\text{sw}}$) at the time of growth
180 (Epstein and Mayeda, 1953). Previous studies have modeled $\delta^{18}\text{O}_{\text{coral}}$ as the linear
181 combination of sea surface temperature (SST) and $\delta^{18}\text{O}_{\text{sw}}$ (e.g., Julliet-Leclerc and
182 Schmidt, 2001; Brown et al., 2006; Thompson et al., 2011), as follows:

$$183 \quad \delta^{18}\text{O}_{\text{coral}} = \delta^{18}\text{O}_{\text{sw}} + a\text{SST} \quad (1)$$

184 where a is a constant which represents the slope between $\delta^{18}\text{O}_{\text{coral}}$ and SST. In this study,
185 the constant was uniformly set to $-0.22\text{‰}/^{\circ}\text{C}$ for all the corals, following Thompson et al.
186 (2011), and we used a model developed by Liu et al. (2013; 2014) to predict $\delta^{18}\text{O}_{\text{sw}}$. The
187 model is an isotopic mass balance model that considers evaporation, precipitation, and
188 mixing with deep ocean water. The coral model uses the monthly output of the isotope-
189 enabled GCM as its input, except for the isotope ratio of deep ocean water, which was
190 obtained from observation-based gridded data compiled by LeGrande and Schmidt et al.
191 (2006). After the model calculates the monthly $\delta^{18}\text{O}_{\text{coral}}$, it is arithmetically averaged to
192 provide the annual $\delta^{18}\text{O}_{\text{coral}}$.

193 The isotope ratio in tree-ring cellulose ($\delta^{18}\text{O}_{\text{tree}}$) was calculated using a model
194 developed by Roden et al. (2000). In this model, $\delta^{18}\text{O}_{\text{tree}}$ is determined by the isotopic
195 composition of the source water used by trees for photosynthesis, and evaporative
196 enrichment on leaves via transpiration. In this study, the value of the isotopic composition



197 in the source water was arbitrarily assumed to be the moving average, traced three-months
198 backward, of the isotopic composition in precipitation at the site. Again, the model used
199 the monthly output of the isotope-enabled GCM as its input. After performing the tree-
200 ring model calculation, the monthly output was weighted using climatological net primary
201 production (NPP) to calculate the annual average. The NPP data were obtained from the
202 US National Aeronautics and Space Administration (NASA) Earth Observation website
203 (<http://neo.sci.gsfc.nasa.gov>).

204 Because the isotopic compositions of the proxies were simulated using the output of
205 the isotope-enabled GCM, their horizontal resolution was the same as that of the GCM.
206

207 **2.3. Experimental design**

208 **2.3.1. Control experiment**

209 The first experiment served as a control (CTRL) experiment, and used the framework
210 of an OSSE. In the experiment, the “simulation” and the “truth” (nature run) were
211 simulated by the same models, with the same forcing, but with different initial conditions.
212 Because the proxy models were driven by the output of the GCM, the modeled proxies
213 were consistent with the modeled climate from the GCM. Thus, here we describe the
214 experimental design for the GCM. The GCM was driven by observed SST and sea-ice
215 data (HadISST; Rayner et al., 2003), and historical anthropogenic (carbon dioxide,



216 methane, and ozone) and natural (total solar irradiance) forcing factors. The simulation
217 covered the period of 1871–2007 (137 years).

218 Although the simulation period included recent times covered by observational data,
219 we assumed that the only variable that could be obtained was the annual mean of $\delta^{18}\text{O}$ in
220 the proxies. We based this assumption on the fact that we wished to perform the DA for a
221 period in which no direct measurements were available, and there were only climate
222 proxies covering the period. Therefore, the temporal resolutions of the “observations” and
223 “simulations” were also annual, considering the typical temporal resolution of the proxies.

224 Observations were generated by adding Gaussian noise to the truth. The spatial
225 distribution of the observations mimicked that of the proxies. The spatial distributions of
226 each proxy for various periods are mapped in Figure 1. As can be seen from the figure,
227 the distributions and the number of proxies varied with time. However, for the sake of
228 simplicity, the distributions of the proxies were assumed to be constant over time in the
229 CTRL experiment (Figure 1 a). The size of the observation errors will be discussed in
230 Section 2.4.

231 The state vector consisted of five variables; surface air temperature and amount of
232 precipitation, as well as the isotopic composition in precipitation, coral, and tree-ring
233 cellulose. The first three variables were obtained from the isotope-enabled GCM, and the



234 other two variables were obtained from the proxy models driven by the output of the
235 GCM.

236

237 **2.3.2. Real proxy data assimilation**

238 The second (REAL) experiment assimilated proxy data sampled in the real world. To
239 mimic realistic conditions, SST and sea-ice concentration data to be used as model forcing
240 were modified from observational to modeled data. In reality, there were no direct
241 observations available for the target period of the proxy DA. Therefore, to reliably
242 evaluate the feasibility of proxy DA, the first estimate should be constructed using
243 modeled SST, as opposed to observed SST. We used SST data from the historical run of
244 the Coupled Model Intercomparison Project Phase 5 (CMIP5; Taylor et al., 2007) from
245 the atmosphere-ocean coupled version of MIROC5 (Watanabe et al., 2010) obtained from
246 the CMIP5 data server (<https://pcmdi.llnl.gov/search/cmip5/>).

247 Because the experiment was not an OSSE, nature run was not necessary.

248

249 **2.3.3. Sensitivity experiments**

250 Four sensitivity experiments were conducted to test the robustness of the results of
251 the proxy DA. In the first sensitivity experiment (CGCM), the simulation run was



252 constructed from the simulation forced by the modeled SST and sea ice as in the REAL
253 experiment. The other settings for the simulation run were the same as those in the CTRL
254 experiment. The nature run was the same as that of the CTRL experiment. Thus, this
255 experiment investigated how the accuracy of the results was decreased by using the
256 simulated SST.

257 In the second sensitivity experiment (VOBS), the experimental design was the same
258 as that in the CGCM, except for the number of proxies that were assimilated. In the
259 CGCM experiment, the distribution and number of proxies were set to be constant over
260 time, as in the CTRL experiment. In the VOBS experiment, the distribution and number
261 of proxies varied with time to reliably evaluate the results of the REAL experiment
262 relative to those from the CTRL experiment.

263 In the third sensitivity experiment (T2-Assim), the surface temperature added with
264 Gaussian noise was assimilated. The purpose of the experiment was to compare the
265 accuracy of the reconstructed DA with that of the proxy DA. The experimental design
266 was the same as that in the CTRL experiment, except for the variables that were
267 assimilated. The noise was added to consider the uncertainties stemmed from the
268 reconstruction. The size of error was determined by considering the typical signal-to-
269 noise ratio (SNR) values of 0.25 and 0.50 (Mann et al., 2007), as well as a further value



270 of 1.0.

271 The final sensitivity (M08) experiment was used to examine the sensitivity to the
272 observation network. The experimental design was the same as for the CTRL, except for
273 the spatial distribution of the proxy. The proxy network used in the experiment was the
274 same as that of Mann et al. (2008). We assumed that isotopic information was available
275 for all the sites, even when this was not the case. For example, even if only tree-ring width
276 data were available at some of the sites in Mann et al. (2008), in this experiment we
277 assumed that isotopic data recorded in tree-ring cellulose were available at the site. The
278 number of grids containing observations were 108 and 250 for the CTRL experiment and
279 M08 respectively.

280 The experimental designs are summarized in Table 1.

281

282 **2.4. Observation data**

283 We used paleoclimate data archived at the National Oceanic and Atmospheric
284 Administration (NOAA; <https://www.ncdc.noaa.gov/data-access/paleoclimatology-data>)
285 and data used in the PAGES 2k Consortium (2013). Additionally, 22 tree-ring cellulose
286 and 7 ice core data sets were collected separately from published papers. We only used
287 oxygen isotopic data (^{18}O) whose temporal resolution was higher than annual; proxies



288 whose resolution was lower than annual were excluded. The full list of proxies used in
289 this study is given in the Appendix. Following Crespin et al. (2009) and Goosse et al.
290 (2010), all proxy records were first normalized, and then averaged onto a T42 grid box to
291 eliminate model bias and produce a regional grid box composite. To compare the results
292 from each experiment effectively, the assimilated variables were all normalized in both
293 the simulation and nature runs, and in the observations in all the experiments.

294 Errors were added to the truth in a normalized manner to provide the observation. The
295 normalized error was uniformly set to 0.50 for all proxies. This was based on the
296 measurement error of $\delta^{18}\text{O}$ in ice cores being reported to range from 0.05 to 0.2‰ (e.g.,
297 Rhodes et al., 2012; Takeuchi et al., 2014), and the corresponding normalized error
298 (measurement error divided by standard deviation of proxy) then ranges from 0.03 to 0.1,
299 with an average of 0.06. Similarly, the measurement error of $\delta^{18}\text{O}$ in coral ranges from
300 0.03 to 0.11‰ (e.g., Asami et al., 2004; Goodkin et al., 2008), and the corresponding
301 normalized error ranges from 0.24 to 1.1, with an average of 0.53. The measurement error
302 of $\delta^{18}\text{O}$ in tree-ring cellulose ranges from 0.1 to 0.3‰ (e.g., Managave et al, 2011; Young
303 et al, 2015), and the corresponding normalized error ranges from 0.08 to 0.55, with an
304 average of 0.28. In practice, due to the error of representativeness and that in observation
305 operator, it is common to increase the observation errors to ensure that the analysis



306 functions effectively (Yoshimura et al., 2014). Furthermore, the measurement errors were
307 not always available; therefore, a uniform value of 0.5 was used for all the proxies.

308

309 **3. Results from the OSSE**

310 The time series of the first estimation, the analysis, and the real values for $\delta^{18}\text{O}$ in
311 corals are compared as an example in Figure 2 at a location where observational data were
312 available (1°N , 157°W). Because the first estimate was the same for all reconstruction
313 years, it is drawn as horizontal lines. After the assimilation, the analysis agreed well with
314 the real values ($R = 0.96$, $p < 0.001$). This confirmed that the assimilation performed well.
315 We then examined how accurately the other variables were reconstructed by assimilating
316 isotopic information. Figure 2 also shows the time series of surface air temperature and
317 precipitation for the same site. There was a clear agreement between the analysis and the
318 truth for both variables ($R = 0.92$ and 0.88 respectively for temperature and precipitation).
319 This indicated that temperature and precipitation were effectively reconstructed by
320 assimilating isotopic variables at this site. This was because the isotope ratio in corals has
321 a signature not only from temperature as given in Eq. 1, but also precipitation (Liu et al.,
322 2013); the correlation with $\delta^{18}\text{O}_{\text{coral}}$ was -0.88 ($p < 0.001$) for both temperature and
323 precipitation, respectively. This example shows that the isotopic proxy records more than



324 one variable.

325 Figure 3 maps the correlation coefficients between the analysis and the truth for the
326 isotope ratio, temperature, and precipitation for 1970–1999. Because the first estimate
327 was constant over time, the temporal correlation between the first estimate and the real
328 value was zero everywhere. Thus, a positive correlation indicated that the DA improved
329 the simulation.

330 The correlation for $\delta^{18}\text{O}$ in precipitation were high at the observation sites, regardless
331 of the proxy type. This was because $\delta^{18}\text{O}$ in both corals and trees is affected by the isotopic
332 composition in precipitated water derived from sea water or soil water. The correlation
333 for $\delta^{18}\text{O}$ in tree-ring cellulose were also high at the observation sites. On the other hand,
334 the correlation for $\delta^{18}\text{O}$ in corals were generally high at low- to mid-latitudes, and the
335 spatial pattern was similar to that of surface temperature. In contrast, closely correlated
336 areas were restricted to low-latitude for precipitation.

337 How can the spatial distribution of the correlation pattern be explained; i.e., what do
338 the proxies represent? To investigate this question, empirical orthogonal function (EOF)
339 analysis was conducted for the simulated $\delta^{18}\text{O}$ in precipitation, corals, and tree-ring
340 cellulose. Only grids that contained observations were included in the analysis. The
341 variables were centered around their means before the analysis. The data covered the



342 period 1871–2007. The EOF patterns and temporal correlations between surface
343 temperature and the characteristic evolution of EOF, or the principal components (PCs)
344 of the first mode of each proxy are shown in Figure 4.

345 The first mode of $\delta^{18}\text{O}$ in ice core explains 14.3% of the total variance and it is the
346 only significant mode according to the Rule of Thumb (North et al., 1982) (the first and
347 the second mode were indistinguishable). The maximum loadings were in Greenland and
348 Antarctica where temperature has been increasing significantly for the past hundred years.
349 Indeed, the PC1 shows the significant trend and is correlated with global mean surface
350 temperature ($R=0.44$, $p < 0.001$). Therefore, it is legitimate to regard ice core data as a
351 proxy of global temperature as revealed from observation (Schneider and Noone, 2007).

352 The first modes of $\delta^{18}\text{O}$ in corals, and tree-ring cellulose represent ENSO. The
353 explained variance of the first modes of $\delta^{18}\text{O}$ in corals, and tree-ring cellulose was 44.2,
354 and 19.0%, respectively. The maximum loadings occurred in the central Pacific for corals,
355 and Tibet for tree-ring cellulose. The temporal correlation between the PC1s and NINO3
356 index were 0.95, and 0.37 for corals and tree-ring cellulose, respectively. Because the
357 isotopic composition in corals is influenced by sea temperature, it is expected that the
358 $\delta^{18}\text{O}$ in corals from the central Pacific records the ENSO signature. Interestingly, the
359 analysis revealed that the $\delta^{18}\text{O}$ in tree-ring cellulose was also influenced by ENSO; hence,



360 this proxy contributes to the reconstruction of temperature and precipitation over the
361 tropical Pacific. Indeed, many previous studies have reported the link between $\delta^{18}\text{O}$ in
362 tree-ring cellulose and ENSO (Sano et al. 2012; Xu et al. 2011; 2013; 2015). The link was
363 explained as follows by Xu et al. (2011): Numerous studies have associated Indian
364 monsoon rainfall with ENSO (e.g., Rasmusson and Carpenter 1983), albeit the
365 relationship was found to be non-stationary over time (Kumar, 1999). The positive phase
366 of ENSO results in a decrease in summer monsoon rainfall in India, which leads to dry
367 conditions in summer. The decrease in precipitation leads to isotopically-enriched
368 precipitation, and the dry conditions enhance the enrichment of water in leaves.
369 Correspondingly, the $\delta^{18}\text{O}$ in tree-ring cellulose becomes heavier than normal in the
370 positive phase of ENSO. Due to the relationships between the coral and tree-ring cellulose
371 data and ENSO, the correlation coefficient between the analysis and real values for the
372 NINO3 index was as high as 0.95 ($p < 0.001$).

373 Although EOF analysis did not reveal any other significant correlation between PCs
374 and climate indices, climate indices for the North Atlantic Oscillation and Southern
375 Annular Mode calculated using the reconstructed data were significantly correlated with
376 the truth (0.59 and 0.46, respectively).

377



378 **4. Real proxy data assimilation**

379 Based on the results of the idealized experiment described in the previous section, we
380 performed a “real” proxy DA, in which sampled and measured data in the real world were
381 assimilated.

382 The temporal correlation between the analysis and observations for temperature and
383 precipitation are shown in Figure 5 (d, h). The observations were obtained from
384 HadCRUT3 (Brohan et al., 2006) for temperature, and GHCN-Monthly Version 3
385 (Peterson and Vose, 1997).

386 Although the real proxy DA had reasonable accuracy, it was inferior relative to the
387 CTRL experiment. We investigated the cause of the decreased accuracy using the outputs
388 of the sensitivity experiments. The design of the experiments was changed in a stepwise
389 fashion to more realistic conditions of proxy data assimilation from the idealized
390 conditions. The correlations between the analysis and the truth, or the observation, for the
391 experiments are shown in Figure 5. The truths for the CGCM and VOBS experiments
392 were the same as those for the CTRL experiment. The global mean correlation
393 coefficients for temperature and precipitation in the experiments are summarized in
394 Figure 6. Note that the correlation was averaged in the same domain for all the
395 experiments to take into account the differences in representativeness.



396 In the CGCM experiment, the temporal correlations between the analysis and the real
397 values were similar to those in the CTRL experiment for both temperature and
398 precipitation (Figure 5 b, f). This indicates that ENSO and its impacts were well
399 represented in the modeled SST used to construct the “simulation”. Watanabe et al. (2010)
400 reported similar modeled SST and observational values for the amplitude of ENSO
401 measured by the NINO3 index, and the spatial patterns of the temperature and
402 precipitation fields regressed on the NINO3 time series (see Figures 13 and 14 in their
403 report).

404 Because the number of proxies for assimilation differed from that in the CGCM
405 experiment, it was not straightforward to compare the results of the REAL experiment
406 with those of the CGCM experiment. To enable an effective comparison of the results,
407 the same number of proxies were assimilated in the VOBS experiment as in the REAL
408 experiment and the same settings were used as in the CGCM experiment for the other
409 variables. Consequently, the performance of the assimilation of the VOBS experiment
410 was similar to that of the CGCM experiment for 1970–1999. Because the number of
411 proxies for assimilation was similar for this period, the assimilation of the VOBS
412 experiment performed well.

413 When the REAL and VOBS experiments were compared, the correlation coefficients



414 for temperature were significantly decreased over the Indian Ocean, eastern Pacific, and
415 Atlantic Ocean. These areas corresponded to areas of low reproducibility in the coral
416 model (Liu et al, 2014). The effects of sea current and river flow in these areas, which
417 were not included in the coral model, were deemed to be considerable. The reproducibility
418 of $\delta^{18}\text{O}$ in corals in these areas requires improvement to enhance the performance of the
419 assimilation.

420

421 **5. Discussion**

422 **5.1. Comparison with the reconstructed temperature assimilation**

423 Hughes and Ammann (2009) recommended assimilating measured proxy data, as
424 opposed to reconstructed data derived from the proxy data. This subsection compares the
425 results from the CTRL and T2-Assim experiments with three different SNR values. Both
426 experimental frameworks were OSSE, and the observations and reconstructed
427 temperature were assumed to be available for the same sites as in the CTRL experiment.
428 To account for the uncertainty derived from the statistical reconstruction, Gaussian noise
429 was added to the temperature from the nature run to generate the observational values in
430 the T2-Assim experiment in a similar fashion to the CTRL experiment. The SNR of the
431 reconstructed temperature was set to 0.25 and 0.50, which are typical values for proxy



432 records (e.g., Mann et al., 2007). Additionally, we also considered an SNR value of 1.0.

433 Figure 7 shows the spatial distribution of the correlation coefficients for temperature
434 and precipitation between the truth and the analysis for each experiment. The global mean
435 correlation coefficients for temperature (precipitation) were 0.49 (0.29), 0.50 (0.22), 0.39
436 (0.16), and 0.25 (0.10) for the experiments assimilating $\delta^{18}\text{O}$ in proxies, and those
437 assimilating temperature with SNR values of 1.0, 0.50, and 0.25, respectively (Figure 8).

438 The values were higher for the assimilated $\delta^{18}\text{O}$ in proxy than for assimilated temperature,
439 with SNR values of 0.25 and 0.50 for both precipitation and temperature. The temperature
440 was reconstructed slightly accurately by assimilation of temperature with a low noise
441 value (SNR = 1.0) than by assimilation of $\delta^{18}\text{O}$ in the proxies. Although using an SNR =
442 1.0 produced more accurate reconstructed field than the ordinal statistical reconstruction,
443 the superior accuracy of the assimilation of proxy data relative to the assimilation of
444 reconstructed temperature was dependent on the magnitude of the SNR; i.e., the accuracy
445 of assimilation of the reconstructed values was dependent on the quality of the
446 reconstructed data. The quality of the reconstructed data was in turn dependent on the
447 stationarity between the proxies and climate, and the degree to which the proxy was
448 affected by factors other than the variable of interest. Isotope-enabled GCMs (Schmidt et
449 al. 2007; LeGrande and Schmidt. 2009) and observations and models for tree-rings



450 (D'Arrigo et al. 2008; Evans et al. 2014) have demonstrated non-stationarity and non-
451 linearity between proxies and climate. Thus, we cannot expect that a high SNR will be
452 maintained over time. However, stationarity and linearity do not have to be considered if
453 the forward proxy model is well-defined (Hughes and Ammann, 2009). Therefore, the
454 assimilation of proxy data offers a useful tool for the reconstruction of paleoclimate, in
455 which the relationship between the proxies and climate constructed with the present-day
456 conditions does not apply.

457

458 **5.2. Sensitivity to the distribution of the proxies**

459 The accuracy of the proxy DA was relatively low over Eurasia and North America,
460 even in the idealized experiment. It was unclear whether this was because of limitations
461 in the proxy data assimilation or the scant distribution of the proxies. This subsection
462 investigates the reasons for the relatively low reproducibility in these areas by comparing
463 the results of the CTRL and M08 experiments, focusing on North America. The number
464 of grids for which proxy data were available over North America was 11 and 126 for the
465 CTRL and M08, respectively.

466 The results for North America are shown in Figure 9. The figure shows the temporal
467 correlation coefficients between the analysis and the truth for surface air temperature and



468 precipitation. The correlation coefficients were calculated for 1970–1999. The accuracy
469 was high in the area in which the proxies were densely distributed for both variables. The
470 values of the coefficients averaged over the United States (30–50°N, 80–120°W) were
471 0.68 and 0.52 for temperature and precipitation, respectively. Compared to the CTRL
472 experiment, the accuracy was enhanced for both variables. The values of the coefficients
473 were 0.17 and 0.24, respectively, in the CTRL experiment. This implies that the
474 performance of the reconstruction was strongly dependent on the distribution of the proxy
475 data. Taking into consideration that proxy DA can assimilate not only proxy data, but also
476 reconstructed data, proxy DA can take advantage of the use of increasingly large amounts
477 of data. Although it is beyond the scope of this study, the combined use of these data is
478 expected to improve the performance of proxy DA.

479

480 **6. Conclusion**

481 The feasibility of using proxy DA for paleoclimate reconstruction was examined in
482 both idealized and real conditions experiments. The idealized (CTRL) experiment had
483 high accuracy at low latitudes due to the dependency of coral data on temperature and
484 precipitation in these regions, and the correlation between ENSO and $\delta^{18}\text{O}$ in corals in
485 Pacific and tree-ring cellulose in Tibet. We performed additional experiments to examine



486 the robustness of proxy DA. In the first experiment, the simulation run was constructed
487 from a simulation forced by modeled SST and sea ice (CGCM experiment). The
488 experiment examined the extent to which the accuracy of the results was decreased using
489 the simulated forcings. The results showed little difference between the performance of
490 the reconstruction for both the temperature and precipitation fields. This was because
491 ENSO, which is the most important mode for the reconstruction, was well represented in
492 the modeled SST. Finally, real proxy DA was performed, where the simulation run was
493 constructed from the simulation forced by the modeled SST, and the real (observed) proxy
494 data were assimilated into the simulation (REAL experiment). The accuracy of the
495 reconstruction decreased over the Indian Ocean, eastern Pacific, and the Atlantic Ocean,
496 where the reproducibility of the proxy model was lower.

497 The results indicated the need to improve isotope-enabled atmospheric GCM and
498 proxy models. The differences between the CTRL and CGCM experiments were due to
499 the use of misrepresented SST values by the coupled GCM. The differences between the
500 CGCM and VOBS experiments were due to the large number of observations for
501 assimilation. Finally, the differences between the VOBS and REAL experiments were due
502 to the misrepresentation of the atmospheric GCM incorporating isotope and proxy models.
503 The differences were largest between the VOBS and REAL experiments (Figure 6).



504 Although it is difficult at this stage to conclude which model caused the decrease in
505 accuracy, it is necessary to improve the reproducibility of models in these regions, and
506 we will investigate the reproducibility of each model in future studies. Furthermore,
507 accurate models for ice cores that incorporate the entire post-depositional processes
508 should be developed to enable more efficient utilization of all of the data.

509 In addition to model reproducibility, the proxy data may have contributed to the
510 decrease in the accuracy of the proxy DA results by transferring erroneous values. It is
511 possible that the data might not have been representative of the targeted temporal and/or
512 spatial scales. Furthermore, it is also possible that the data were highly distorted by non-
513 climatic factor(s). Thus, a thorough quality control, similar to the procedures used in
514 weather forecasting, should be conducted before assimilation.

515 Although the accuracy of the REAL experiment was decreased compared with the
516 CTRL experiment, it may still be possible to reliably reconstruct ENSO and ENSO-
517 related variations in temperature and precipitation with this proxy network because the
518 correlation coefficient between the analysis and the observations was as high as 0.83 in
519 the REAL experiment. Although the reconstruction of ENSO is dependent on data from
520 corals, and the time span covered by corals is relatively short (a few hundred years),
521 ENSO can still be reliably reconstructed due to its global impact, as was demonstrated in



522 the relationship between isotopes in tree-ring cellulose from Tibet.

523 Moreover, because the reproducibility was heavily dependent on the spatial
524 distribution, we expect that it will increase as more proxy data become available. In this
525 sense, because proxy DA can assimilate both proxy and reconstructed data, the combined
526 use of the two types of data is expected to improve the performance of the assimilation.

527 The DA algorithm used in this study did not consider non-stationarity among proxies
528 and climate variables because the Kalman gain was constant over time. To address non-
529 stationarity, the Kalman gain for a specific reconstruction year should be constructed for
530 several tens of years before and after that year. Furthermore, an ensemble Kalman filter
531 (EnKF) can only capture linear relationships between observations and the modeled state.
532 The use of other algorithms should be investigated in future studies for scenarios where
533 non-linearity is not negligible. Thus, it is important in future studies to investigate non-
534 stationarity and non-linearity among proxies and climate variables to identify suitable
535 algorithms for proxy DA.

536

537 7. Acknowledgements

538 The first author was supported by the Japan Society for the Promotion of Science (JSPS)
539 via a Grant-in-Aid for JSPS Fellows. This study was supported by the Japan Society for
540 the Promotion of Science Grants 15H01729, 26289160, and 23226012, the SOUSEI
541 Program, the ArCS project of MEXT, Project S-12 of the Japanese Ministry of the



542 Environment, and the CREST program of the Japan Science and Technology Agency.

543



544 **8. References**

- 545 Annan, J. D. and Hargreaves, J. C., Identification of climatic state with limited proxy data,
546 *Clim. Past*, 8, 1141-1151, 2012.
- 547 Asami, R., Yamada, T., Iryu, Y., Meyer, C. P., Quinn, T. M., and Paulay, G., Carbon and
548 oxygen isotopic composition of a Guam coral and their relationships to
549 environmental variables in the western Pacific, *Palaeogeogr Palaeoclimatol*, 212, 15, 1-22,
550 2004.
- 551 Bhend, J., Franke, J., Folini, D., Wild, M., and Brönnimann, S., An ensemble-based
552 approach to climate reconstructions, *Clim. Past*, 8, 963-976, 2012.
- 553 Brohan, P., Kennedy, J. J., Harris, I., Tett, S. F. B., and Jones, P. D., Uncertainty estimates
554 in regional and global observed temperature changes: A new data asset from 1850,
555 *J. Geophys. Res.* 111, D12106, 2006.
- 556 Brown, J., Simmonds, I., and Noone, D., Modeling $\delta^{18}\text{O}$ in tropical precipitation and the
557 surface ocean for present-day climate, *J. Geophys. Res.*, 111, D05105, 2006.
- 558 Crespin, E., Goosse, H., Fichefet, T., and Mann, M., The 15th century Arctic warming in
559 coupled model simulations with data assimilation, *Clim. Past*, 5, 389-401, 2009.
- 560 D'Arrigo, R., Wilson, R., Liepert, B., and Cherubini, P., On the 'Divergence Problem' in
561 Northern Forests: A review of the tree-ring evidence and possible causes, *Global
562 Planet. Change*, 60, 289-305, 2008.
- 563 Dee, S., Emile-Geay, J., Evans, M., Allam, A., Steig, E., and Thompson, D., PRYSM: An
564 open-source framework for PROXY System Modeling, with applications to oxygen-
565 isotope systems, *Journal of Advances in Modeling Earth Systems*, 7, 1220-1247,
566 2015.
- 567 Dirren, S. and Hakim, C., Toward the assimilation of time-averaged observations,
568 *Geophys. Res. Lett.*, 32, L04804, 2005.
- 569 Dubinkina, S. and Goosse, H., An assessment of particle filtering methods and nudging
570 for climate state reconstructions, *Clim. Past*, 9, 1141-1152, 2013.
- 571 Epstein, S., and Mayeda, T., Variation of O^{18} content of waters from natural sources,
572 *Geochimica Cosmochim. Ac.*, 4, 213-224, 1953.
- 573 Evans, M. N., Tolwinski-Ward, S. E., Thompson, D. M., and Anchukaitis, K. J.,
574 Applications of proxy system modeling in high resolution paleoclimatology,
575 *Quaternary Sci. Rev.*, 76, 16-28, 2013.
- 576 Evans, M. N., Smerdon, J. E., Kaplan, A., Tolwinski-Ward, S. E., and González-Rouco,
577 J. F., Climate field reconstruction uncertainty arising from multivariate and
578 nonlinear properties of predictors, *Geophys. Res. Lett.*, 41,



- 579 doi:10.1002/2014GL062063, 2014.
- 580 Gaspari, G., and Cohn, S., Construction of correlation functions in two and three
581 dimensions, *Q. J. Roy. Meteor. Soc.*, 125, 723-757, 1999.
- 582 Goodkin, N. F., Hughen, K. A., Curry, W. B., Doney, S. C., and Ostermann, D. R., Sea
583 surface temperature and salinity variability at Bermuda during the end of the Little
584 Ice Age, *Paleoceanography*, 23, PA3203, 2008.
- 585 Goosse, H., Renssen, H., Timmermann, A., Bradley, R., and Mann, M., Using
586 paleoclimate proxy-data to select optimal realisations in an ensemble of simulations
587 of the climate of the past millennium, *Clim. Dyn.*, 27, 165-184, 2006.
- 588 Goosse, H., Crespin, E., de Montety, A., Mann, M., Renssen, H., and Timmermann, A.,
589 Reconstructing surface temperature changes over the past 600 years using climate
590 model simulations with data assimilation, *J. Geophys. Res.*, 115, D09108, 2010.
- 591 Goosse, H., Crespin, E., Dubinkina, S., Loutre, M., Mann, M., Renssen, H., Sallaz-Damaz,
592 Y., Shindell, D., The role of forcing and internal dynamics in explaining the
593 “Medieval Climate Anomaly”, *Clim. Dyn.*, 39, 2847-2866, 2012.
- 594 Hoffmann, G., Werner, M., Heimann, M., Water isotope module of the ECHAM
595 atmospheric general circulation model: A study on timescales from days to several
596 years, *J. Geophys. Res.*, 103, D1427, 16871-16896, 1998.
- 597 Hughes, M., and Ammann, C., The future of the past -an earth system framework for high
598 resolution paleoclimatology: editorial essay, *Climatic Change*, 94, 247-259, 2009.
- 599 Huntley, H., and Hakim, G., Assimilation of time-average observations in a quasi-
600 geostrophic atmospheric jet model, *Clim. Dyn.*, 35, 995-1009, 2010.
- 601 Joussaume, S., Sadourny, R., and Jouzel, J., A general circulation model of water isotope
602 cycles in the atmosphere, *Nature*, 311, 24-29, 1984
- 603 Jouzel, J., Russell, G. L., Suozzo, R. J., Koster, R. D., White, J. W. C., and Broecker, W.
604 S., Simulations of the HDO and H₂¹⁸O Atmospheric cycles using the NASA GISS
605 General Circulation Model: The seasonal cycle for present-day conditions, *J.*
606 *Geophys. Res.*, 92, D12, 14739-14760, 1987.
- 607 Julliet-Leclerc, A., and Schmidt, G., A calibration of the oxygen isotope
608 paleothermometer of coral aragonite from Porites, *Geophys. Res. Lett.*, 28, 21, 4135-
609 413, 2001.
- 610 Kumar, K., Rajagopalan, B., Cane, M. A., On the weakening relationship between the
611 Indian Monsoon and ENSO, *Science*, 284, 2156, 1999.
- 612 Lee, J.-E., Fung, I., DePaolo, D., and Henning, C., Analysis of the global distribution of
613 water isotopes using the NCAR atmospheric general circulation model, *J. Geophys.*
614 *Res.*, 112, D16306, 2007.



- 615 LeGrande, A., and Schmidt, G., Global gridded data set of the oxygen isotopic
616 composition in seawater, *Geophys. Res. Lett.*, 33, L12604, 2006.
- 617 LeGrande, A., and Schmidt, G., Sources of Holocene variability of oxygen isotopes in
618 paleoclimate archives, *Clim. Past*, 441-455, 2009.
- 619 Liu, G., Kojima, K., Yoshimura, K., Okai, T., Suzuki, A., Oki, T., Siringan, F., Yoneda, M.,
620 and Kawahata, H., A model-based test of accuracy of seawater oxygen isotope ratio
621 record derived from a coral dual proxy method at southeastern Luzon Island, the
622 Philippines, *J. Geophys. Res-Biogeol.*, 118, 853-859, 2013.
- 623 Liu, G., Kojima, K., Yoshimura, K., and Oka, A., Proxy interpretation of coral-recorded
624 seawater ^{18}O using 1-D model forced by isotope-incorporated GCM in tropical
625 oceanic regions, 119, doi: 10.1002/2014JD021583, 2014.
- 626 Managave, S. R., Sheshshayee, M. S., Ramesh, R., Borgaonkar, H. P., Shad, S. K.,
627 Bhattacharyya, A., Response of cellulose oxygen isotope values of teak trees in
628 differing monsoon environments to monsoon rainfall, *Dendrochronologia*, 29, 89-
629 97, 2011.
- 630 Mann, M., Rutherford, S., Wahl, E., and Ammann, C., Robustness of proxy-based climate
631 field reconstruction methods, 112, D12109, 2007.
- 632 Mann, M., Zhang, Z., Hughes, M., Bradley, R., Miller, S., Rutherford, S., Ni, F., Proxy-
633 based reconstructions of hemispheric and global surface temperature variations over
634 the past two millennia, *P. Natl. Acad. Sci. USA.*, 105, 13252-13257, 2008.
- 635 Mathiot, P., Goosse, H., Crosta, X., Stenni, B., Braida, M., Renssen, H., Van Meerbeeck,
636 C. J., Masson-Delmotte, V., Mairesse, A., and Dubinkina, S., Using data assimilation
637 to investigate the causes of Southern Hemisphere high latitude cooling from 10 to 8
638 ka BP, *Clim. Past*, 9, 887-901, 2013.
- 639 Noone, D. and Simmonds, I., Associations between $\delta^{18}\text{O}$ of water and climate parameters
640 in a simulation of atmospheric circulation for 1979-95, *J. Climate*, 15, 3150-3169,
641 2002.
- 642 North, G., Bell, T. L., and Cahalan, R. F., Sampling errors in the estimation of empirical
643 orthogonal functions, *Mon. Weather Rev.*, 110, 699-706, 1982.
- 644 Okazaki, A., and Yoshimura, K., Development of stable water isotope incorporated
645 atmosphere-land coupled model MIROC5, in prep.
- 646 PAGES 2k Consortium, Continental-scale temperature variability during the past two
647 millennia, *Nat. Geosci.*, 6, 339-346, 2013.
- 648 Peterson, T. C., and Vose, R. S., An overview of the global historical climatology network
649 temperature database, *B. Am. Meteorol. Soc.*, 78, 2837-2849, 1997.
- 650 Rasmusson, E. M., and Carpenter, T. H., The relationship between eastern Equatorial



- 651 Pacific sea surface temperatures and rainfall over India and Sri Lanka, *Mon. Weather*
652 *Rev.*, 111, 517-528, 1983.
- 653 Rayner, N. A., Parker, D. E., Horton, E. B., Folland, C. K., Alexander, L. V., Rowell, D.
654 P., Kent, E. C., Kaplan, A., Global analyses of sea surface temperature, sea ice, and
655 night marine air temperature since the late nineteenth century, *J. Geophys. Res.*, 108,
656 D144407, 2003.
- 657 Rhodes, R. H., Bertler, N. A. N., Baker, J. A., Steen-Larsen, H. C., Sneed, S. B.,
658 Morgenstern, U., and Johnsen, S. J., Little Ice Age climate and oceanic conditions
659 of the Ross Sea, Antarctica from a coastal ice core record, *Clim. Past*, 8, 1223-1238,
660 2012.
- 661 Risi, C., Bony, S., Vimeux, F., and Jouzel, J., Water-stable isotopes in the LMDZ4 general
662 circulation model: Model evaluation for present-day and past climates and
663 applications to climatic interpretations of tropical isotopic records, *J. Geophys. Res.*,
664 115, D12118, 2010.
- 665 Roden, J., Lin, G., and Ehleringer, J., A mechanistic model for interpretation of hydrogen
666 and oxygen isotope ratios in tree-ring cellulose, *Geochim. Cosmochim. Ac.*, 64, 21-
667 35, 2000.
- 668 Sano, M., Xu, C., and Nakatsuka, T., A 300-year Vietnam hydroclimate and ENSO
669 variability record reconstructed from tree ring $\delta^{18}\text{O}$, *J. Geophys. Res.* 117, D12115,
670 2012.
- 671 Schmidt, G., Hoffmann, G., Shindell, D., and Hu, Y., Modeling atmospheric stable
672 isotopes and the potential for constraining cloud processes and stratosphere-
673 troposphere water exchange, *J. Geophys. Res.*, 110, D21314, 2005.
- 674 Schmidt, G., LeGrande, A., and Hoffmann, G., Water isotope expressions of intrinsic and
675 forced variability in coupled ocean-atmosphere model, *J. Geophys. Res.*, 112,
676 D10103, 2007.
- 677 Schneider, D. P. and Noone, D. C., Spatial covariance of water isotope records in a global
678 network of ice cores spanning twentieth-century climate change, *J. Geophys. Res.*,
679 112, D18105, 2007.
- 680 Schotterer, U., Stichler, W., Ginot, P., The influence of post-depositional effects on ice
681 core studies: Examples from the Alps, Andes, and Altai, in *Earth Paleoenvironments:*
682 *Records Preserved in Mid- and Low-Latitude Glaciers*, pp.39-59, Kluwer Acad,
683 Dordrecht, The Netherlands, 2004
- 684 Steiger, N., Hakim, G., Steig, E., Battisti, D., and Roe, G., Assimilation of Time-Averaged
685 Pseudoproxies for Climate Reconstruction, 27, 426-441, 2014.
- 686 Taylor, K. E., Stouffer, R. J., Meehl, G., An overview of CMIP5 and the experiment



- 687 design, *B. Am. Meteor. Soc.*, 93, 485-498, 2007.
- 688 Takeuchi, N., Fujita, K., Aizen, V. B., Narama, C., Yokoyama, Y., Okamoto, S., Naoki,
689 K., and Kobota, J., The disappearance of glaciers in the Tien Shan Mountains in
690 Central Asia at the end of Pleistocene, *Quaternary Sci. Rev.*, 103, 26-33, 2014.
- 691 Thomposon, D. M., Ault, T. R., Evans, M. N., Cole, J. E., and Emile-Geay, J., Comparison
692 of observed and simulated tropical climate trends using a forward model of coral
693 $d^{18}O$, *Geophys. Res. Lett.*, 38, L14706, 2011.
- 694 van der Schrier, G. and Barkmeijer, J., Bjerknes' hypothesis on the coldness during
695 AD1790-1820 revisited, *Clim. Dyn.*, 25, 537-553, 2005.
- 696 von Storch, H., Cubasch, U., Gonzalez-Rouco, J. F., Jones, J. M., Voss, R., Widmann, M.,
697 and Zorita, E., Combining paleoclimatic evidence and GCMs by means of data
698 assimilation through upscaling and nudging (DATUN), *Proc. 11th Symposium on*
699 *Global Climate Change Studies*, AMS Long Beach, CA, 2000.
- 700 Watanabe, M., Suzuki, T., O'ishi, R., Komuro, Y., Watanabe, S., Emori, S., Takemura, T.,
701 Chikira, M., Ogura, T., Sekiguchi, M., Takata, K., Yamazaki, D., Yokohota, T.,
702 Nozawa, T., Hasumi, H., Tatebe, H., and Kimoto, M., Improved climate simulation
703 by MIROC5: Mean States, Variability, and Climate Sensitivity, 23, 6312-6335, 2010.
- 704 Werner, M., Langebroek, P., Carlsen, T., Herold, M., and Lohmann, G., Stable water
705 isotopes in the ECHAM5 general circulation model: Toward high-resolution isotope
706 modeling on a global scale, *J. Geophys. Res.*, 116, D15109, 2011.
- 707 Widmann, M., Goosse, H., van der Schrier, G., Schnur, R., and Barkmeijer, J., Using data
708 assimilation to study extratropical Northern Hemisphere climate over the last
709 millennium, *Clim. Past*, 6, 627-644, 2010.
- 710 Xu, C., Sano, M., and Nakatsuka, T., Tree ring cellulose $\delta^{18}O$ of *Fokienia hodginsii* in
711 northern Laos: A promising proxy to reconstruct ENSO?, *J. Geophys. Res.* 116,
712 D245109, 2011.
- 713 Xu, C., Zheng, H., Nakatsuka, T., and Sano, M., Oxygen isotope signatures preserved in
714 tree ring cellulose as a proxy for April-September precipitation in Fujian, the
715 subtropical region of southeast China, *J. Geophys. Res.-Atmos.*, 118, 12805-12815,
716 2013.
- 717 Xu, C., Pumijumnong, N., Nakatsuka, T., Sano, M., Li, Z., A tree-ring cellulose $\delta^{18}O$ -
718 based July-October precipitation reconstruction since AD 1828, northwest Thailand,
719 *J. Hydrol.*, 529, 422-441, 2015.
- 720 Yoshimura, K., Kanamitsu, M., Noone, D., and Oki, T., Historical isotope simulation
721 using Reanalysis atmospheric data, *J. Geophys. Res.*, 113, D19108, 2008.
- 722 Yoshimura, K., Miyoshi, T., and Kanamitsu, M., Observation system simulation



723 experiments using water vapor isotope information, *J. Geophys. Res.*, 119, 7842-
724 7862, 2014.

725 Young, G. H. F., Loader, N. J., McCarroll, D., Bale, R. J., Demmler, J. C., Miles, D.,
726 Nayling, N., Rinne, K. T., Robertson, I., Watts, C., and Whitney, M., Oxygen stable
727 isotope ratios from British oak tree-rings provide a strong and consistent record of
728 past changes in summer rainfall, *Clim. Dyn.*, 45, 3609-3622, 2015.

729

730



731

Tables

732 **Table 1.** Experimental designs. The observation network used in the CTRL experiment is
 733 denoted as Orig.

	SST data to drive simulation run	SST data to drive truth run	Assimilated variable	Observation network	Missing data
CTRL	HadISST	HadISST	Simulated $\delta^{18}\text{O}$	Orig	w/o missing
CGCM	Modeled SST	HadISST	Simulated $\delta^{18}\text{O}$	Orig	w/o missing
VOBS	Modeled SST	HadISST	Simulated $\delta^{18}\text{O}$	Orig	w/ missing
REAL	Modeled SST	-	Observed $\delta^{18}\text{O}$	Orig	w/ missing
T2-Assim	HadISST	HadISST	Simulated T2	Orig	w/o missing
M08	HadISST	HadISST	Simulated $\delta^{18}\text{O}$	M08	w/o missing

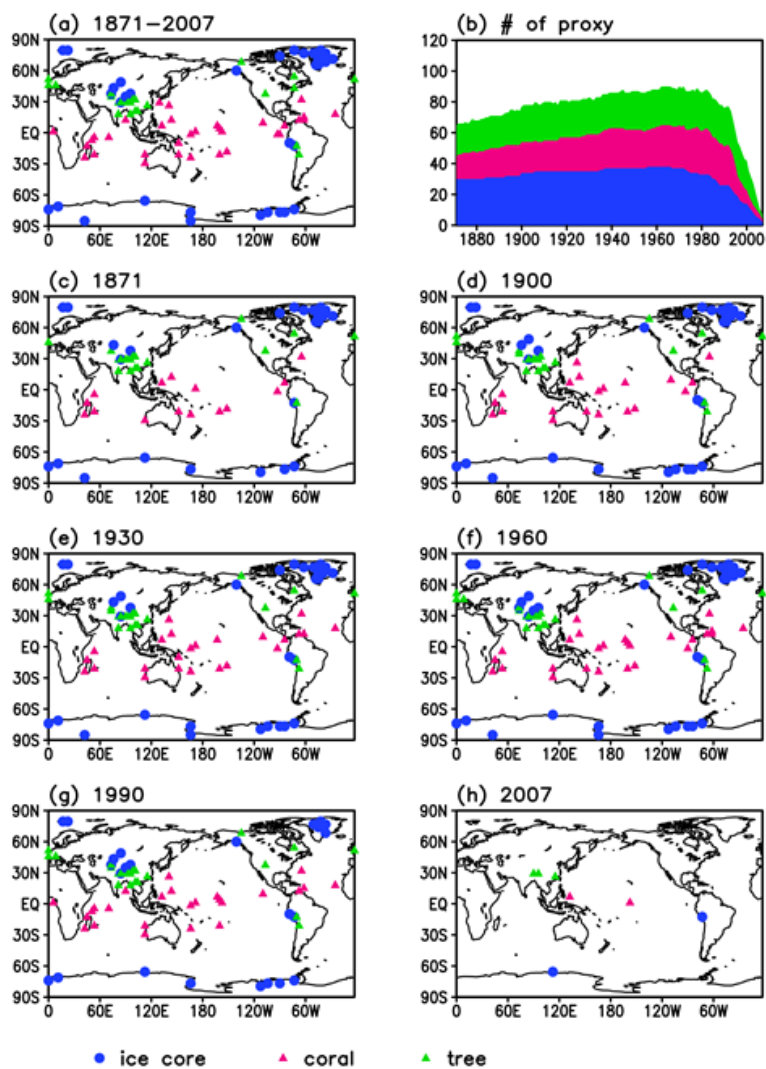
734

735



736

Figures



737

738 **Figure 1**

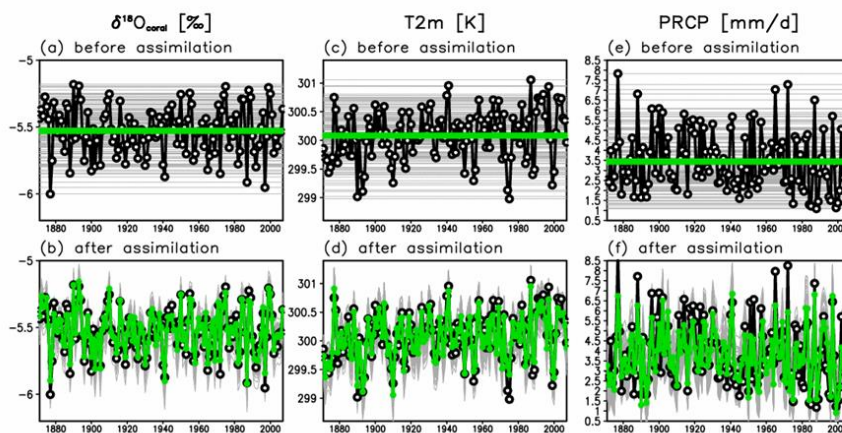
739 Spatial distribution of proxies ($\delta^{18}\text{O}$ in ice cores, corals, and tree-ring cellulose, denoted
 740 by blue, pink, and green, respectively). (a) Proxies spanning at least one year during
 741 1871–2000 are mapped (b) The number of proxies is depicted as a function of time. (c–



742 h) The spatial distributions of the proxies are mapped for (c) 1871, (d) 1900, (e) 1930, (f)

743 1960, (g) 1990, and (h) 2007.

744



745

746

Figure 2

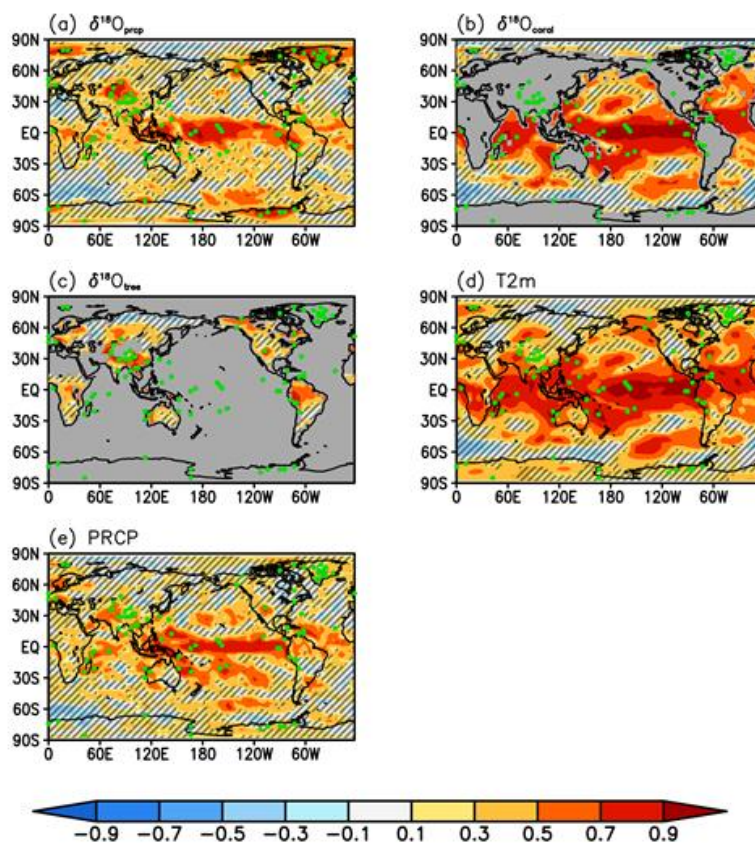
747

748

749

750

Annual mean $\delta^{18}\text{O}$ in corals at a location where observational data were available (1°N , 157°W) for (a) background and (b) analysis. The black line indicates the truth, gray lines indicate ensemble members, and green line indicates the ensemble mean.

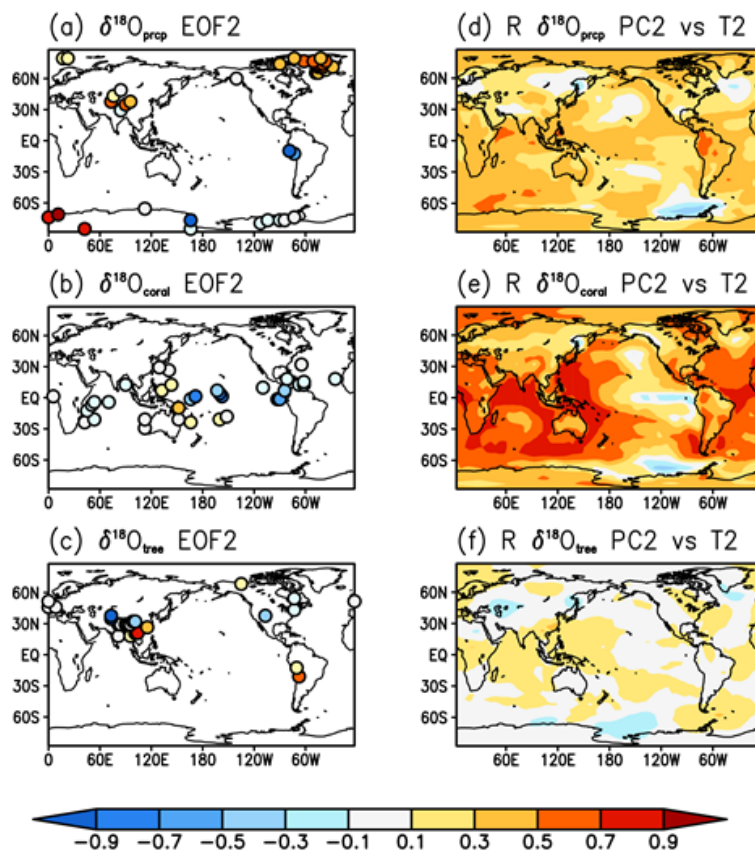


751

752 **Figure 3**

753 Temporal correlation between the analysis and the truth. The green dot represents the
754 location of the proxy sampling site. The hatched area indicates where the correlation is
755 not statistically significant ($p > 0.05$).

756

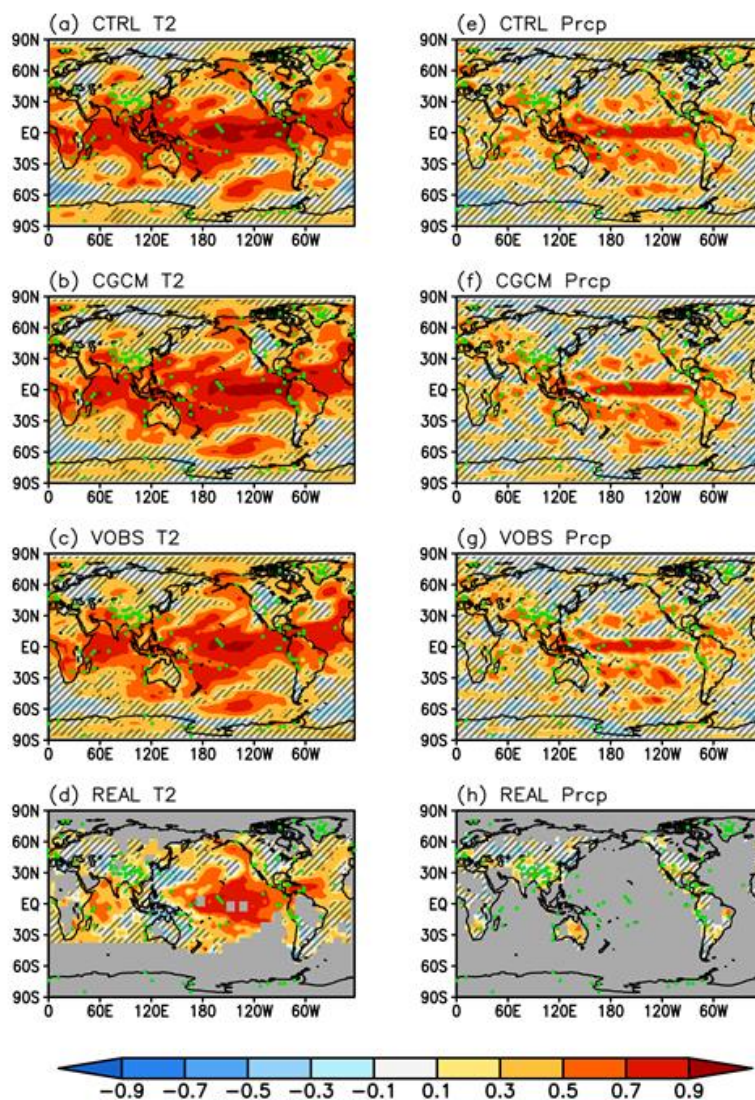


757

758 **Figure 4**

759 First mode of EOF and the correlation between PC1 and temperature for (a and d) ice
760 cores, (b and e) corals, and (c and f) tree-ring cellulose.

761

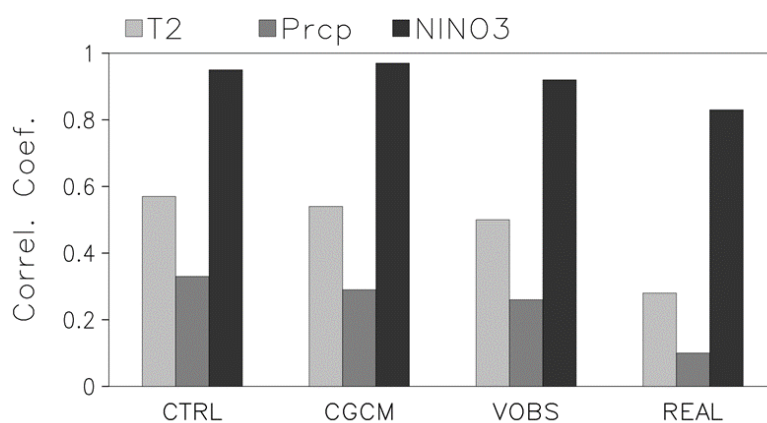


762

763 **Figure 5**

764 Temporal correlation between the analysis and the truth for (a–d) temperature and (e–h)
765 precipitation, for each experiment. The green dot represents the location of the proxy
766 sampling site. The hatched area indicates where the correlation is not statistically
767 significant ($p > 0.05$).

768

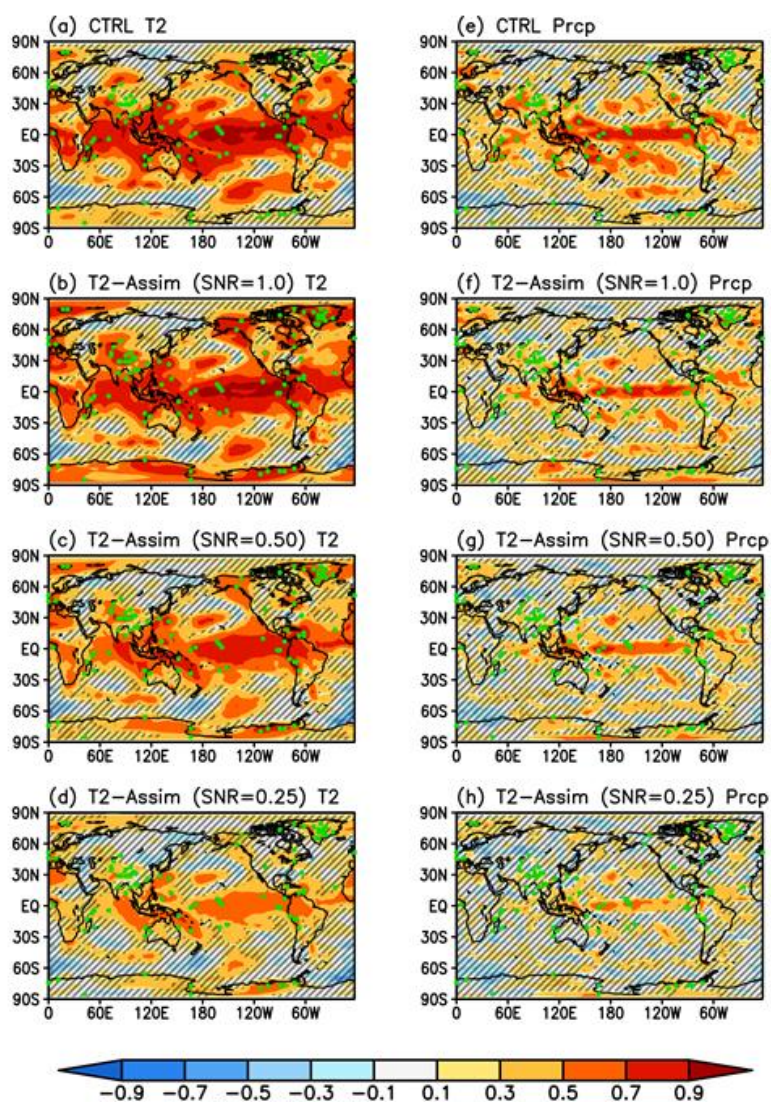


769

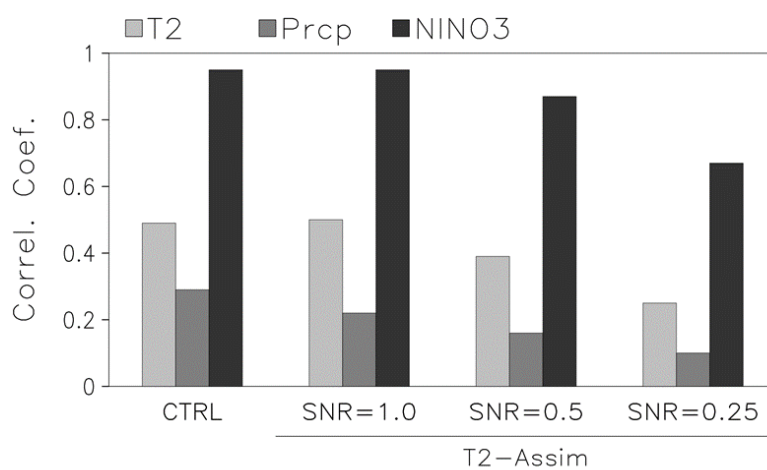
770 **Figure 6**

771 Temporal correlation between the analysis and the truth for each experiment for 1970–
772 1999. The values for temperature and precipitation are the global mean of the temporal
773 correlations.

774



775
776 **Figure 7**
777 Temporal correlations between the analysis and the truth for (a–d) temperature and (e–h)
778 precipitation, for (a and e) CTRL and (b–d and f–h) T2-Assim. The green dot represents
779 the location of the proxy sampling site. The hatched area means that the correlation is not
780 statistically significant ($p > 0.05$).
781

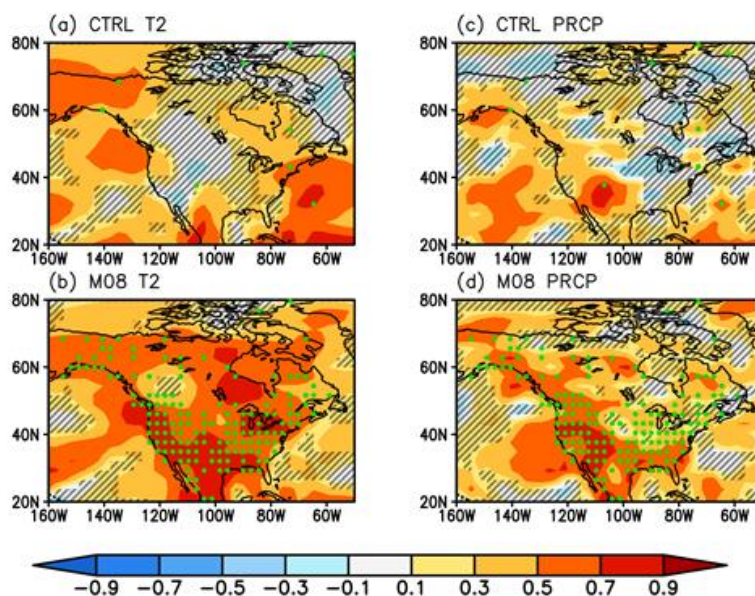


782

783 **Figure 8**

784 Temporal correlation between the analysis and the truth for each experiment for 1970–
785 1999. The values for temperature and precipitation are the global mean of the temporal
786 correlations.

787



788

789 **Figure 9**

790 Temporal correlations in North America between the analysis and the truth for (a–d)
791 temperature, and (e–h) precipitation, for experiments using different proxy networks. The
792 green dot represents the location of the proxy sampling site. The hatched area indicates
793 where the correlation is not statistically significant ($p > 0.05$).